



## CORRIGENDUM

# Slamming forces during water entry of a simple harmonic oscillator – CORRIGENDUM

John T. Antolik, Jesse L. Belden, Nathan B. Speirs and Daniel M. Harris<sup>†</sup>

doi:10.1017/jfm.2023.820, Published by Cambridge University Press, 6 November 2023

The authors recently discovered an error in (3.7) which is corrected below:

$$\ddot{x}_n = \frac{d}{dt} \left[ \frac{1}{\alpha M + m} \int_0^t k(x_b - x_n) d\tau \right] - \frac{\alpha^2 M^2 V^2}{(\alpha M + m)^3} \frac{dm}{dx_n} - \frac{\alpha M V}{(\alpha M + m)^3} \frac{dm}{dx_n} \int_0^t k(x_b - x_n) d\tau. \quad (\text{C3.7})$$

The last term in the equation was previously omitted. In the limit where  $\alpha M \gg m$ , this term vanishes so the conclusions of the paper and the one-way coupled model presented in (3.9) and (3.10) (and associated predictions throughout) are unaffected by this error. In fact, this term accounts for some of the previous underprediction of the two-way coupled model compared to the experimental results and thus slightly improves the agreement between the experiments and model in the range of experimental parameters explored. As such, we have reproduced figures 3(d), 4, 8 and 9 below using the corrected equations for the two-way coupled model. As  $\alpha M$  and  $m$  become closer in magnitude (for instance, with a lightweight nose or a larger nose radius), the influence of this missing term becomes more pronounced.

<sup>†</sup> Email address for correspondence: [daniel\\_harris3@brown.edu](mailto:daniel_harris3@brown.edu)

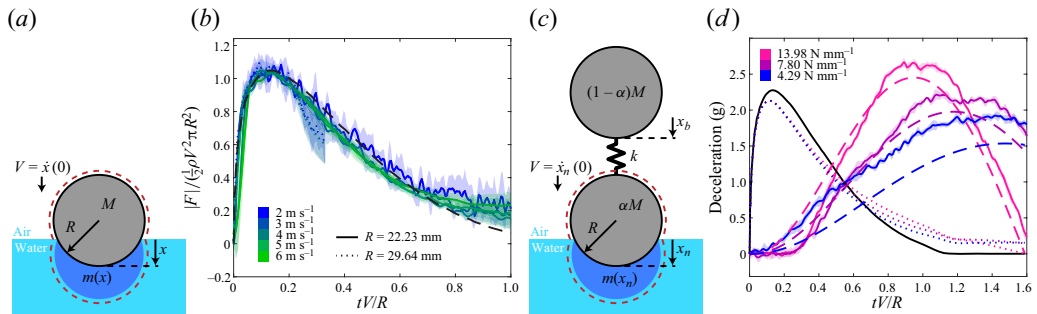


Figure 3. (a) Schematic of the rigid added-mass model. The impinging body must accelerate an effective mass  $m(x)$  of fluid as it enters the water; hence the impact force can be obtained from an expression of momentum conservation for the outlined system. (b) The force from rigid impact experiments at several speeds with different nose radii ( $R = 22.23, M = 0.578 \text{ kg}$  or  $R = 29.64, M = 0.537 \text{ kg}$ ) collapse onto a single curve when using an inertial scaling. The Shiffman and Spencer  $C_F$  curve (dashed line) agrees excellently with the experiments. The shaded regions around the experimental curves indicate standard deviation of at least three trials with the lower speed experiments exhibiting greater variation between trials due to the lower signal-to-noise ratio. The nose used for the  $R = 29.64 \text{ mm}$  rigid experiments is not a complete hemisphere so the data is truncated accordingly (importantly, the peak force is captured accurately). (c) We extend the classic added-mass model to the case of a flexible impactor by introducing a trailing spring and mass. The outlined system for which we write conservation of momentum now includes the external contribution from the spring. (d) The deceleration of the flexible impactor body measured in experiments (solid coloured lines,  $V = 4 \text{ m s}^{-1}$ ,  $R = 22.23 \text{ mm}$ ,  $\alpha = 0.12$ ,  $M = 0.592 \text{ kg}$ ) is captured well by the flexible added-mass model (dashed lines). Furthermore, the model predicts that the deceleration of the impactor centre of mass (dotted lines) deviates only slightly from the rigid theoretical  $C_F$  curve (solid black line), suggesting that the elasticity does not have a strong influence on the hydrodynamics in this regime. The shaded region around the experimental curves indicates the standard deviation between five trials.

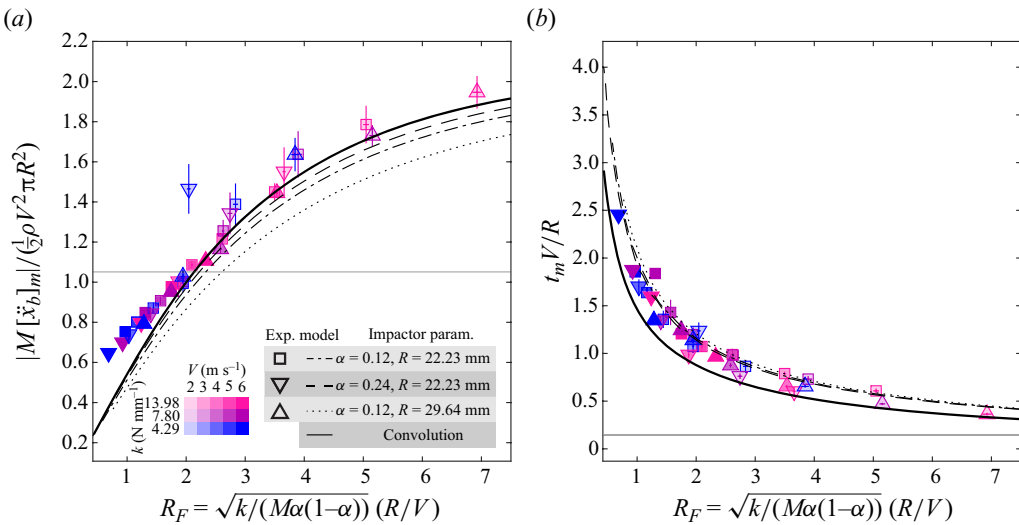


Figure 4. The scaled maximum impact force (a) and the time of the peak force (b) collapse along a single curve against the hydroelastic number  $R_F$  for experiments in which the impact speed, stiffness, nose radius and mass ratio are varied. The error bars, which are sometimes smaller than the marker size, show the standard deviation between at least three trials. The simplified prediction from the convolution integral in (3.17) (solid black lines) agrees well with the experiments (markers) and captures the critical hydroelastic factor near  $R_F \approx 2$  at which the peak force in the flexible case equals the peak force in the equivalent rigid case (horizontal line). The marker shape indicates the impactor mass ratio and nose radius in a given experiment while the colour and opacity indicate the stiffness and impact speed, respectively. The two-way coupled added mass model from (3.7) and (3.8) is also shown, which more accurately predicts the time of the peak force. The two-way model line style (dashed, dotted or dash-dotted) indicates the mass ratio and nose radius corresponding to a particular predicted curve as shown in the legend.

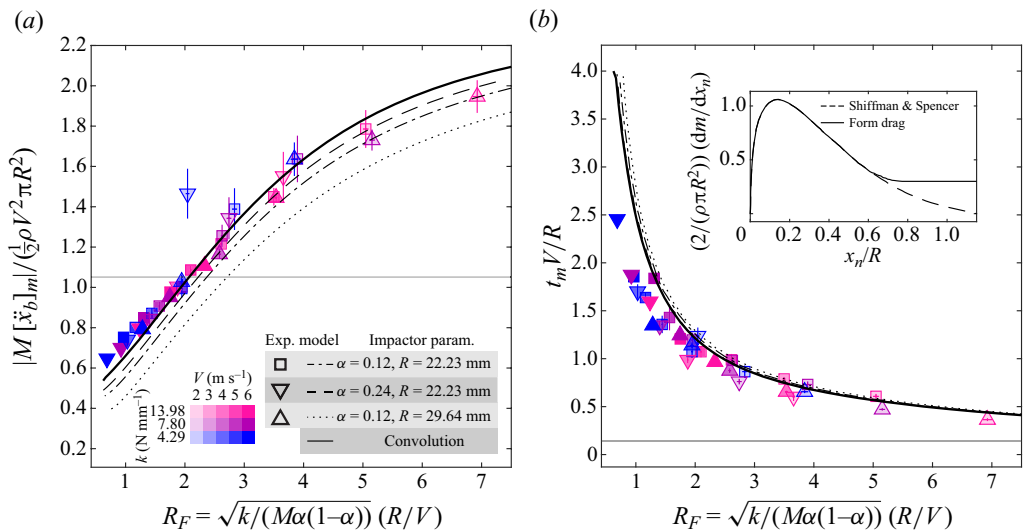


Figure 8. The scaled maximum impact force (a) and the time of the peak force (b) are plotted against the hydroelastic factor  $R_F$  and compared with our model which is updated to include form drag. The error bars, which are sometimes smaller than the marker size, show the standard deviation between at least three experimental trials. The marker shape indicates the impactor mass ratio and nose radius in a given experiment while the colour and opacity indicate the stiffness and impact speed, respectively. The simplified prediction from the convolution integral in (3.17) is shown in the solid black lines and the two-way coupled added-mass model from (3.7) and (3.8) is also shown. The two-way model line style (dashed, dotted or dash-dotted) indicates the mass ratio and nose radius corresponding to a particular predicted curve as shown in the legend. The agreement with the theory improves compared to figure 9 when we update the added-mass function  $dm/dx$  to include the contribution of form drag as shown in the inset panel in (b).

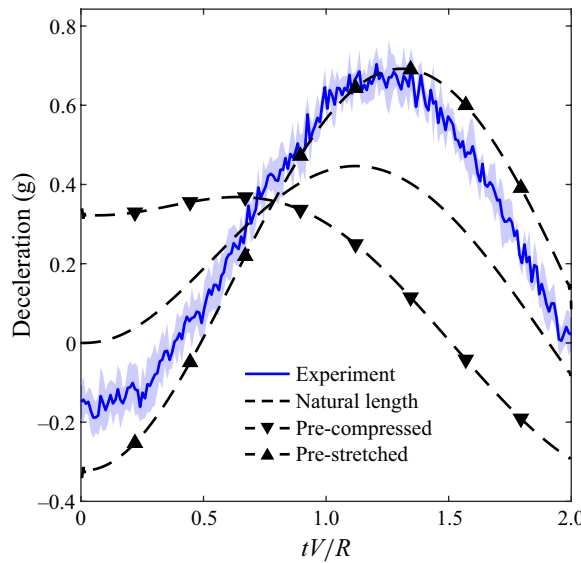


Figure 9. The experimental acceleration curve (solid blue line) with  $\alpha = 0.24$ ,  $V = 2 \text{ m s}^{-1}$  and  $k = 4.29 \text{ N mm}^{-1}$  is compared to the theoretical prediction of the two-way flexible added-mass model (dashed lines). The shaded region represents the standard deviation of three experimental trials. The natural length curve corresponds to the impact model with no pre-load while the pre-stretched or pre-compressed curves are generated by modifying the initial conditions of the model with  $\delta(0) = \pm 0.39 \text{ mm}$  and  $\dot{\delta}(0) = 0$ . This initial displacement corresponds to the estimated free-fall oscillation amplitude based on the weight of the hanging nose and spring stiffness. The experimental curve closely matches the pre-stretched case suggesting that  $\delta(0) < 0$  for these experiments. The peak deceleration is notably increased for this case compared to the theoretical curve with no pre-load.